Precisely Enumerating Circulating Tumor Cells Utilizing Multi-functional Microfluidic Chip and Unique Image Interpreting Algorithm

Mingxing Zhou[1,2‡], Hui Zheng[1‡], Zhaoba Wang[2‡], Ren Li[1], Xiaoran Liu[3], Weikai Zhang[1], Zihua Wang[1], Huiping Li[3*], Zewen Wei[1*], Zhiyuan Hu[1,4,5*]

[1] CAS Key Laboratory of Standardization and Measurement for Nanotechnology，CAS Key Laboratory for Biomedical Effects of Nanomaterials and Nanosafety, CAS Center for Excellence in Nanoscience, National Center for Nanoscience and Technology of China, Beijing 100190, China;

[2] School of Information and Communication Engineering, North University of China, Taiyuan 030051, China;

[3] Key Laboratory of Carcinogenesis and Translational Research (Ministry of Education), Department of Breast Oncology, Peking University Cancer Hospital & Institute, Beijing 100142, China;

[4] Sino-Danish College, University of Chinese Academy of Sciences, Beijing 100049, China;

[5] Yangtze River Delta Academy of Nanotechnology and Industry Development Research, Jiaxing 314000, China.

[‡] These authors contributed equally to the work.

[*] Corresponding Authors: Zhiyuan Hu (huzy@nanoctr.cn)，Huiping Li (huipingli2012@hotmail.com) or Zewen Wei (weizw@nanoctr.cn).

Supplementary Figure S1
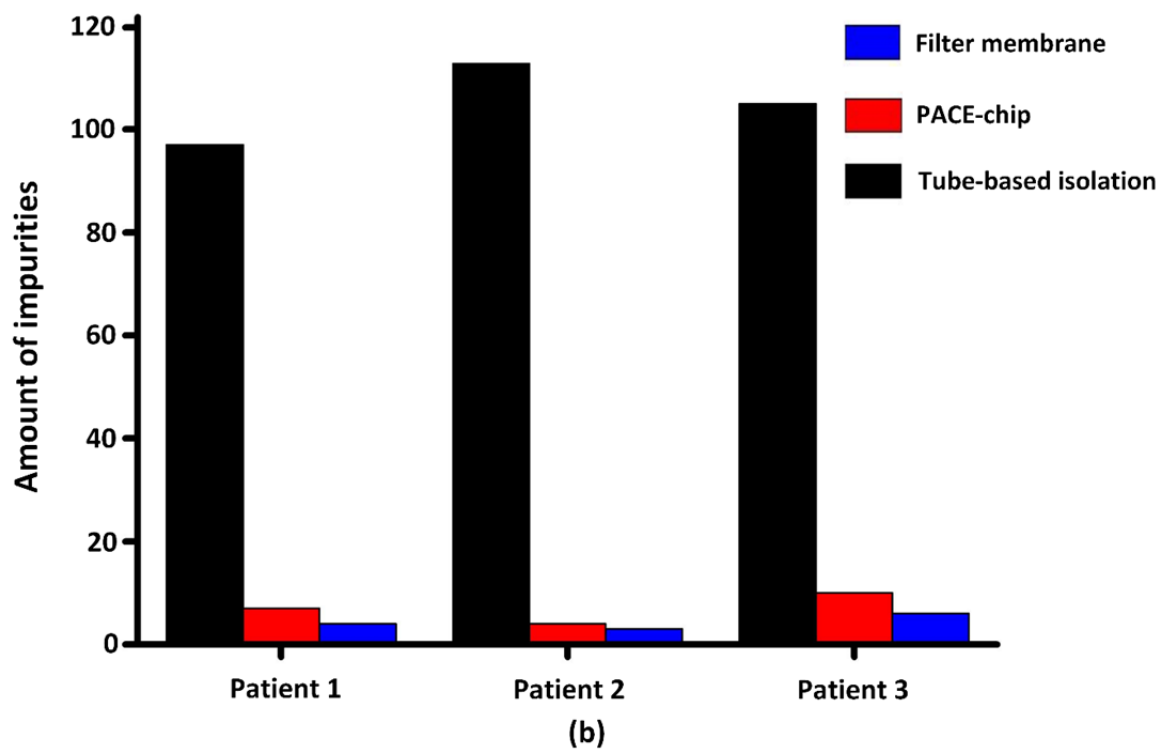
Micro-valve parameters
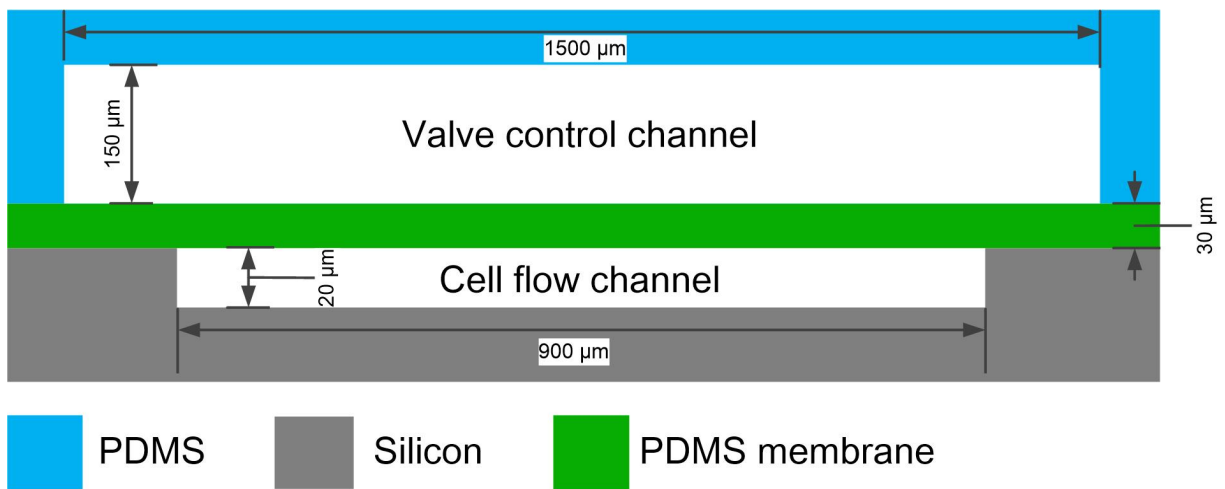
A typical micro valve in which a PDMS membrane, which controlled by the air in the valve control channel, was used as valve film to control the cell movement in the cell flow channel.

Supplementary Figure S2

Blood impurities filtered by micro-pillars
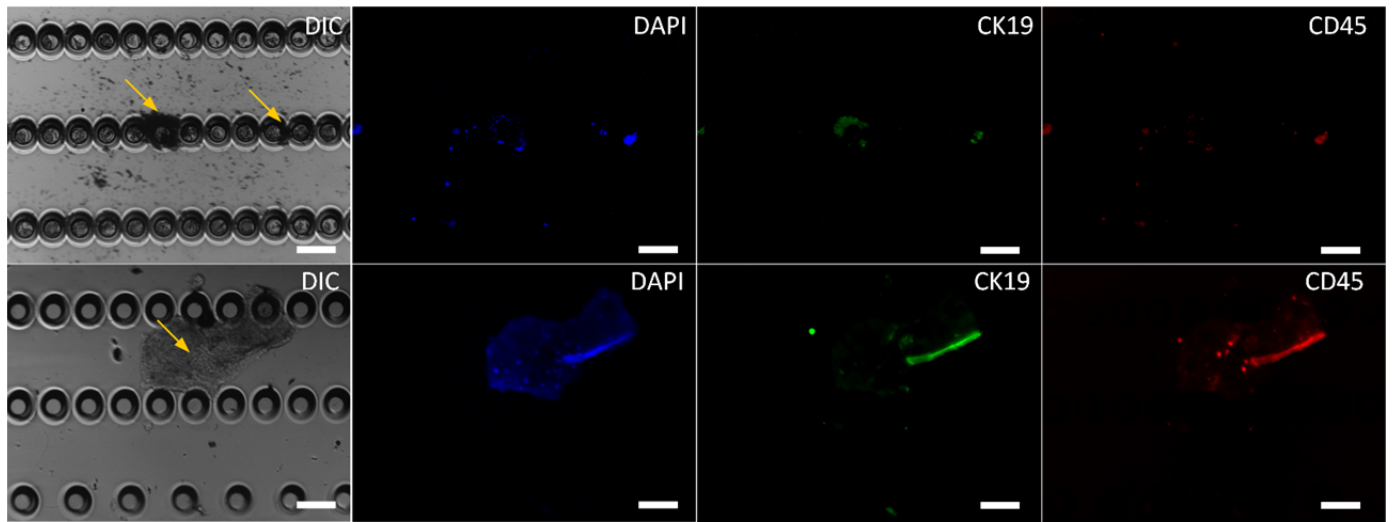
(a)

(b)

The yellow arrows in S1a indicate impurities existing in whole blood which exhibit diverse profiles and dimensions. To avoid possible jamming in microfluidic channel, impurities larger than 32 μm were filtered. To achieve optimum filtering efficiency, 1500 micro-pillars were fabricated in the blood filtering segment. The distances between adjacent pillars are 100, 50 and 32 μm respectively. While pumping 2 mL blood into the microfluidic channel with a flow rate of 120 μL/Min.

Most impurities stay in the filtering segment. To evaluate if there were any CTCs being kept in this area, which may compromise the enumeration accuracy, we stained this area with DAPI, CK19-FITC and CD45-PE. It turns out all impurities exhibits broad spectrum fluorescence while no CTC which should be CD45 negative, DAPI and CK19 positive[1-3] was found in this area. Scale bars were all 100 μm.

To quantitatively evaluate the efficiency of eliminating impurities, we used two methods (PACE chip and a filter membrane with 30 μm diameter holes, Type H22247, Puyihua, China) to filter 1 mL patient bloods. The filtered bloods were collected for centrifuging at 2000 rpm for 5 minutes. After removing the supernatant, the products of centrifuge were re-suspended with 10 μL PBS, stained with DAPI, CK19-FITC and CD45-PE and dropped on a glass slide to recognize remained impurities larger than 100 μm in filtered blood which were manually counted. Another 1 mL unfiltered blood which experienced the whole tube-based CTC isolation process (protocol described in experimental section) was treat with the same method and used as control. The results (Figure b) demonstrate that our chip eliminates over 95% impurities, compared with unfiltered blood in tube.

Moreover, we monitored the cell loss while filtering the blood impurities. In the blood filtering segment, after filtering 2 mL patient blood, DAPI, CD45 and CK19 were used to stain any cell left in this segment. Few (less than 200) cells were kept in this part, compared with huge cell numbers (more than 10^6 cells) in 2 mL blood, the cell loss in the blood filtering segment is ignorable (less than 0.02 %).

Patient information:

All patients are female breast cancer patients. In detail: Patient 1: 66 years old, Stage IIIc, receiving first-line chemotherapy; Patient 2: 58 years old, Stage IV, receiving multi-metastases at first-treatment; Patient 3: 62 years old, Stage IIb, receiving second-line chemotherapy.

Supplementary Figure S3

Measurement of magnetic field strength


(a)

(b)
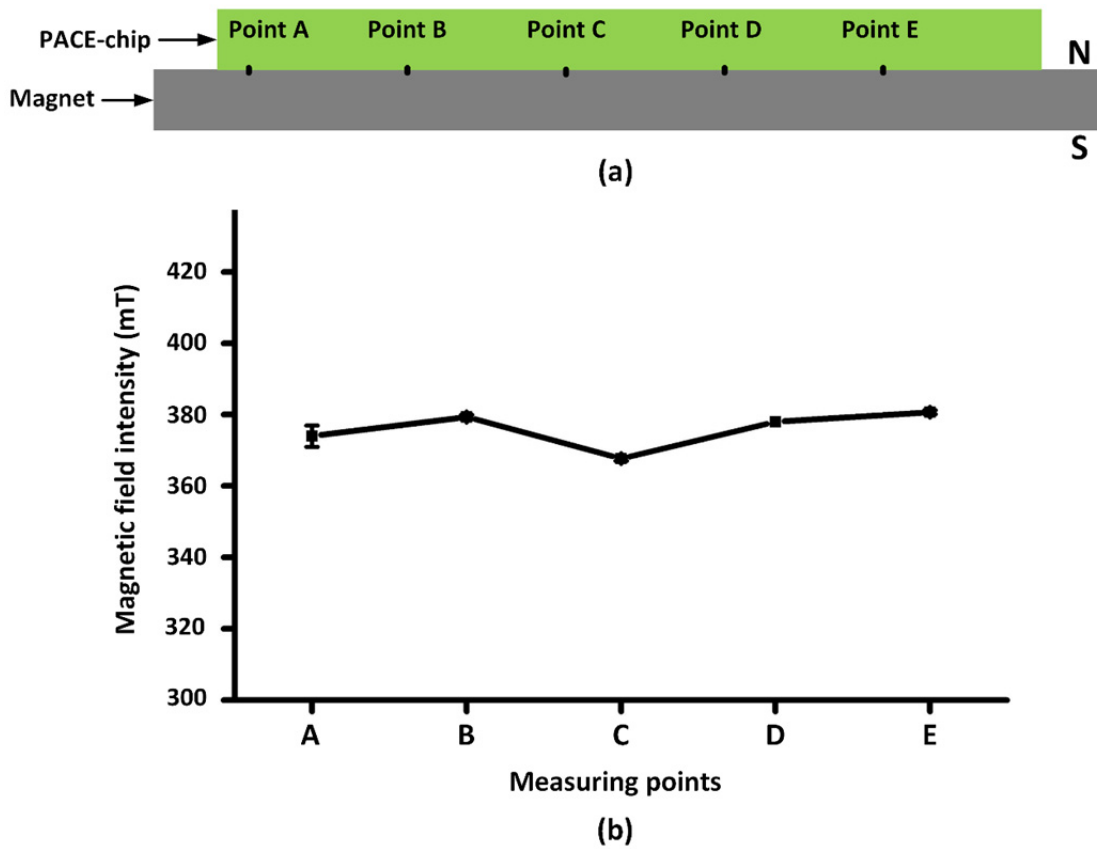
To isolate EpCAM positive cells in the blood sample, an NbFeB permanent magnet (50 mm X 50 mm X 25mm) was placed under the cell isolating segment (schemed as Figure a) with N pole upwards and S pole downwards. We measured the magnetic field strength of 5 points, using a digital gaussmeter (HT20, Hengtong, China). Figure b indicated that the magnetic field intensities in 5 points were evenly distributed, ranging from 370 mT to 380 mT.

Supplementary Figure S4

The simulation of the flow velocity distribution in a gradually-widened channel
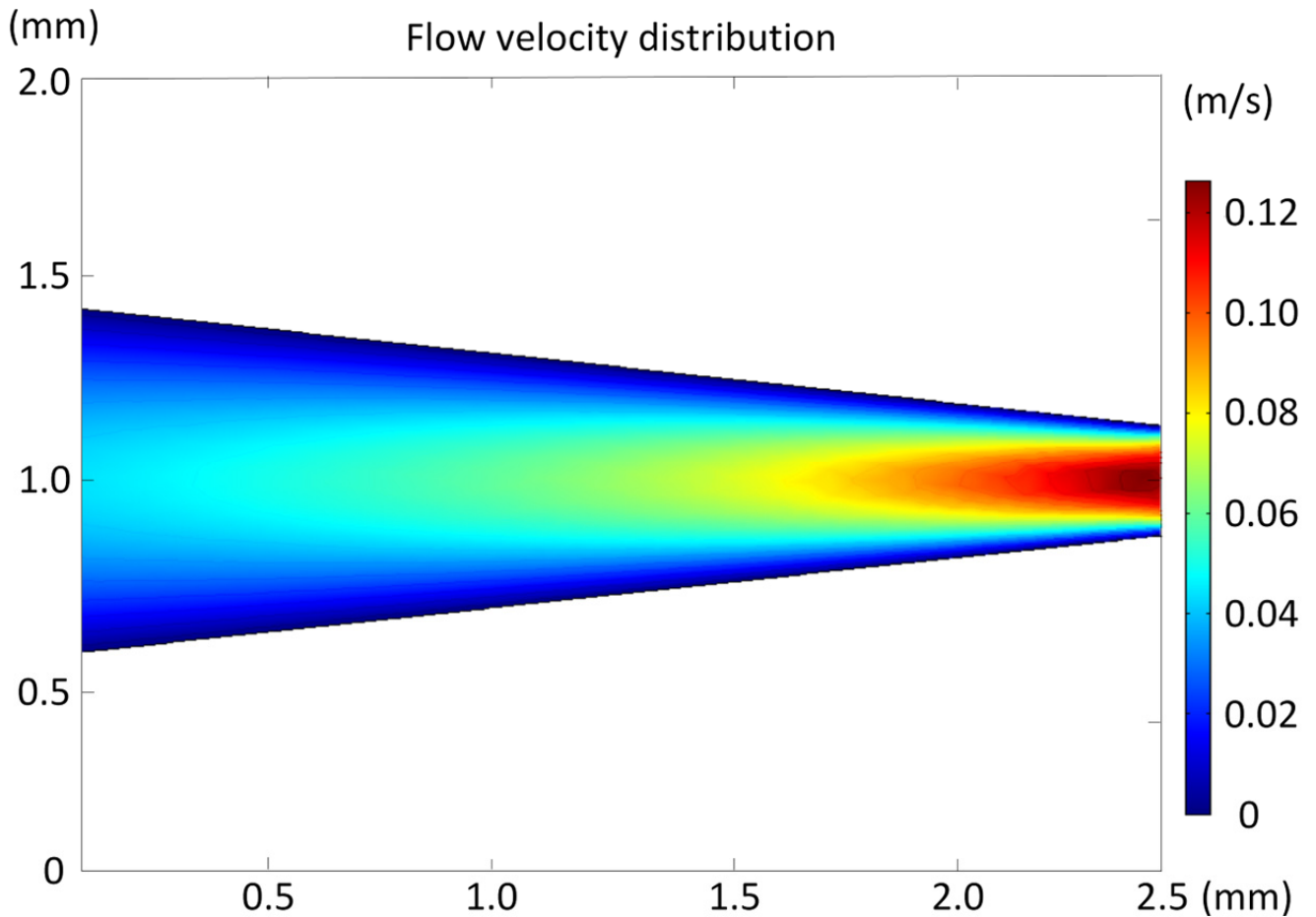
A FEA software Comsol V5.0 was used to analyze the flow velocity distribution in the gradually-widened micro fluidic channel. The channel length and depth are 2.5 mm and 20 μm, respectively, while the inlet (right) and outlet (left) are respectively 0.25 and 0.85 mm in width. In this simulation, the flow velocity at input (right) was set at 0.13 m/s to fit our experiment. According to the simulation results, velocity decreased gradually from 0.13 m/s at input to 0.04 m/s at output.

Supplementary Figure S5

Cell distributions in different parts of the gradually-widened micro fluidic channel


(a)

(b)
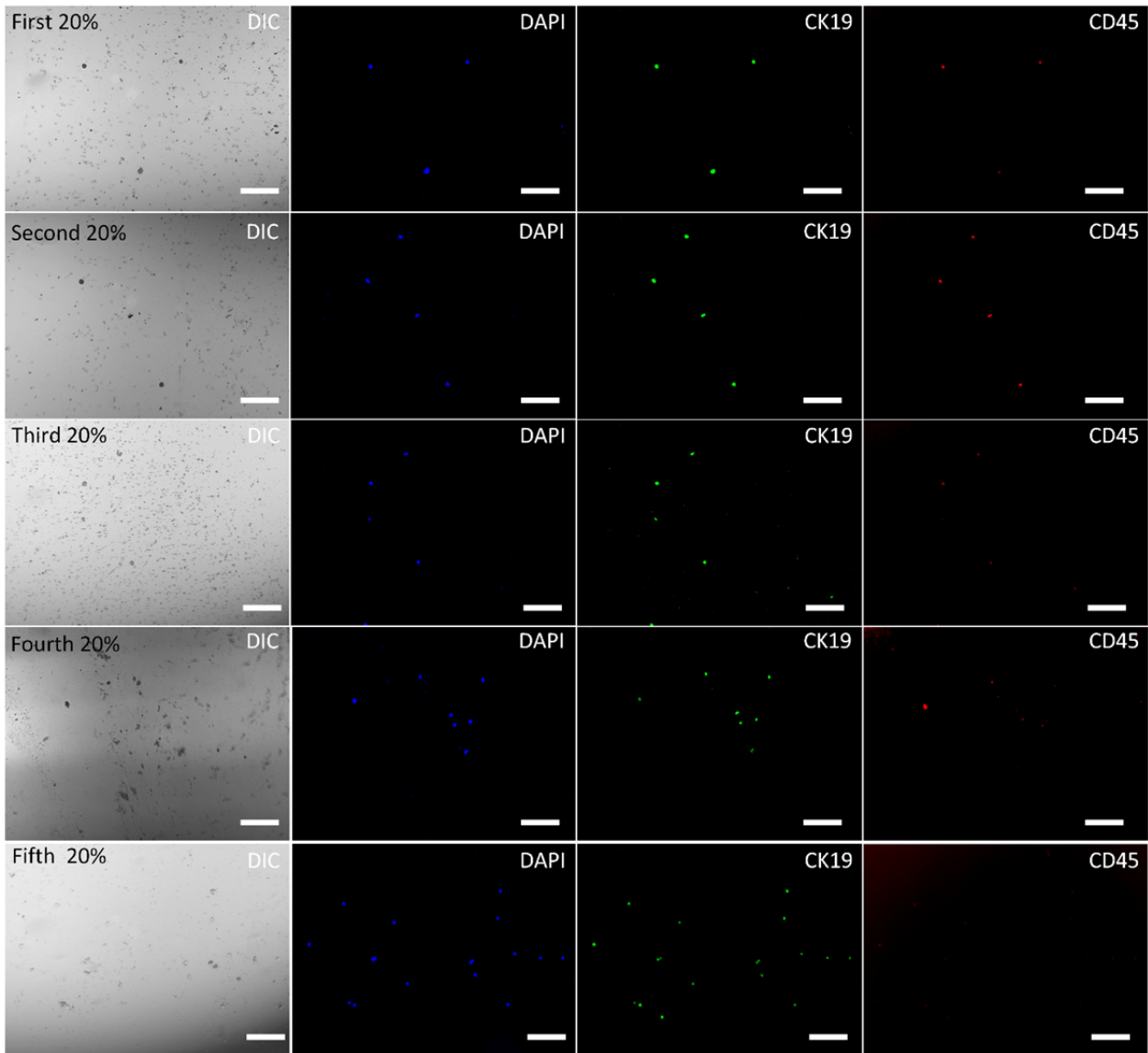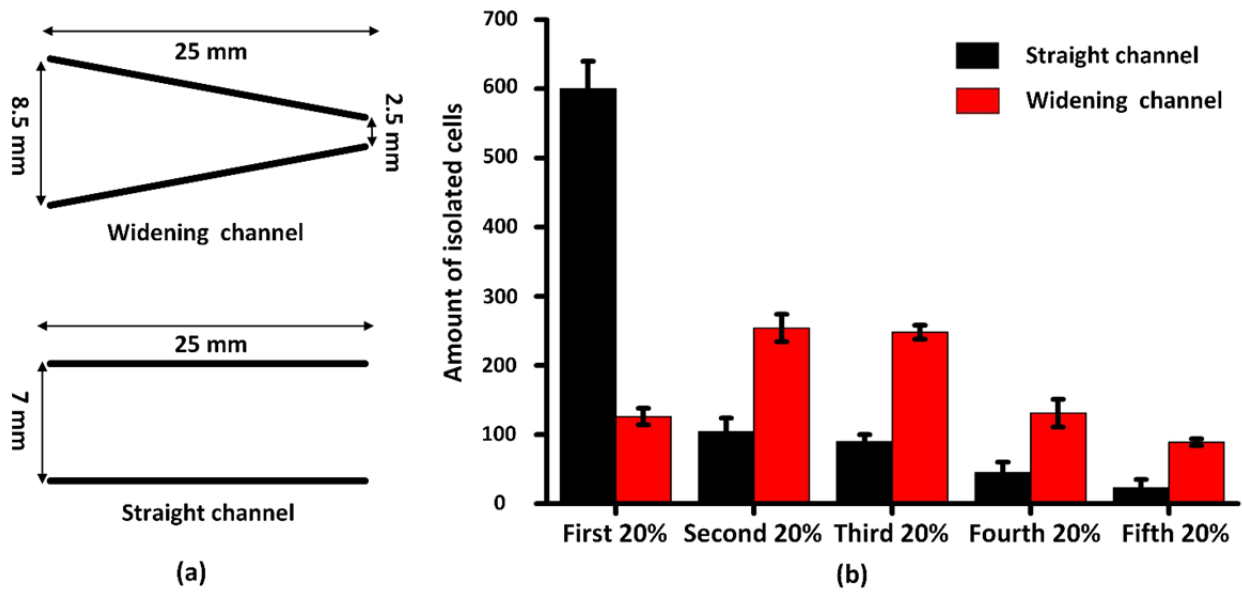
(c)

To adapt the situation that cell are labelled with different amount of magnetic beads, a gradually-widened micro fluidic channel was designed to avoid channel jamming and better cell isolation efficiency by gradually weakening the flow velocity and related drag force. Ideally, cells with more magnetic beads would be captured in the front of the channel, while cells with fewer magnetic beads would be captured in the rear of the channel.

We quantitatively analysed the distribution of isolated cells in a gradually-widened channel and a straight rectangle channel. The depth of both channel is 20 μm, other dimensions are showed in Figure a. 1000 SKBR-3 cells were firstly incubated with 10 μL immuno-magnetic beads conjugated with EpCAM antibody for 30 minutes, and then were pumped into both channels. The flow rate was 120 μL/Min. The isolated cells were stained with DAPI, fluorescently imaged and counted. We divided both channels respectively into 5 parts (first 20%, second 20%, third 20%, fourth 20% and fifth 20%) from channel inlet to outlet for cell distribution determination. The results were showed in Figure b. As expected, all isolated cells distributed relatively even in five parts of the gradually-widened channel, while most isolated cells distributed in the front of the straight rectangle channel. 17% cells were lost in this segment. Data are expressed as the mean ± SD from 3 independent assays.

We further verified this design with 2 mL clinical blood sample. After incubation with 10 μL immuno-magnetic beads conjugated with EpCAM antibody for 30 minutes, we diluted the blood to 5 mL and pumped them into the microfluidic chip. Before flowing into the gradually-widened isolating channel for cell isolating, the blood was filtering by the micro-pillar array. Then we immuno-stained all cells with DAPI, CK19-FITC and CD45-PE. Figure c indicated isolated cells distributions in five parts of the channel, which fit the data in Figure b. No cell aggregation or channel jam was observed. Images were all taken at 10X lens (Axio Imager A2, Carl Zeiss, Germany). Scale bars were 100 μm.

Supplementary Figure S6

## The optimization of the spacing between adjacent V-shaped microstructures
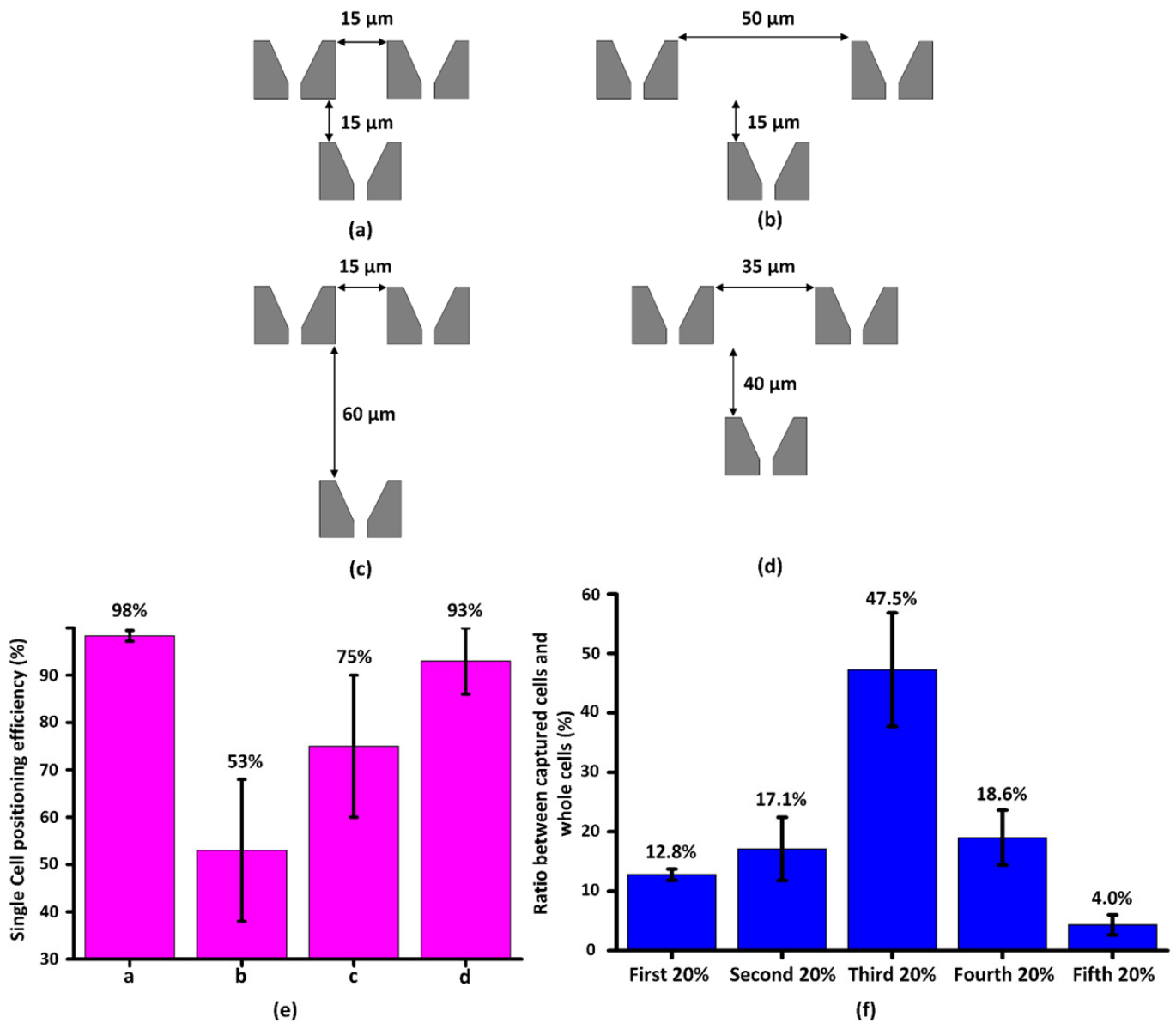
To achieve optimum single-cell positioning efficiency and avoid channel jamming, we tested 4 different arrangements of the V-shaped microstructures. We pumped 100 µL SKBR-3 cell solution (10^4 cells/mL) into the channel at 40 µL/Min. After finishing cell positioning, all cells were stained by DAPI and fluorescently imaged. Cells were counted by analyzing the image by ImageJ[TM] from NIH. The single cell positioning efficiency was calculating by diving captured cells by total pumped cells. According to the positioning efficiency in Figure e, results of each arrangement and its corresponding efficiency are: (a) Both the row spacing and column spacing were 15 µm. The average positioning efficiency was up to 98%, but the channel was jammed seriously. (b) The row

spacing was 50 μm and column spacing was 15 μm. No jamming was observed, however the average positioning efficiency was only 53%. (c) The row spacing was 15 μm and column spacing was 60 μm. The average positioning efficiency was 75%. Meanwhile, the channel was still easy to be jammed. (d) The row spacing was 35 μm and column spacing was 45 μm. The average positioning efficiency was 93%, and no jamming was observed. For CTC enumerating it is critical to simultaneously realize a positioning efficiency as high as possible and a jamming-free flow. Therefore, 35 μm row spacing and 45 μm column spacing were finally taken as the optimum numbers. Based on the optimal spacing design, we divided the single cell positioning segment into 5 parts (first 20%, second 20%, third 20%, fourth %20 and fifth 20%) from inlet to outlet and tested the positioned cells distribution in these parts. The results in Figure f showed that over 96% of positioned cells distributed in the first 4 parts. Less than 3% cells were lost in this segment. Data are expressed as the mean ± SD from 3 independent assays.

Supplementary Figure S7

Isolating spiked cells from blood

(a)

(b)
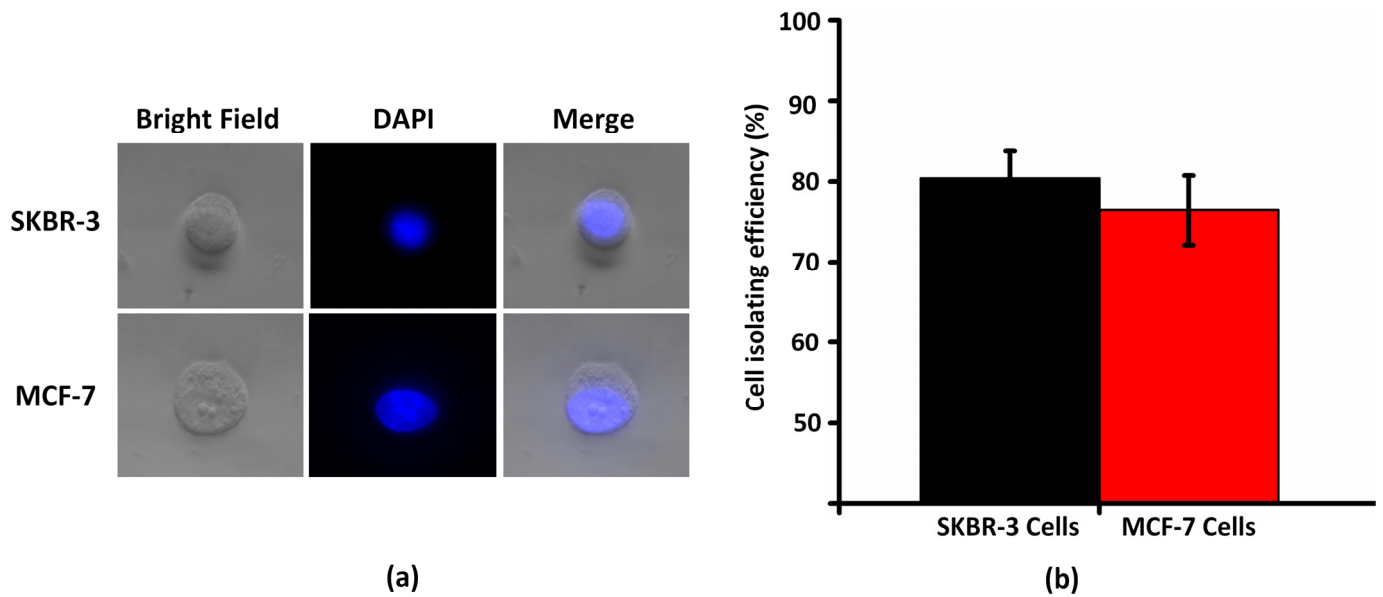
Firstly, 100 DAPI-stained SKBR-3 cells (Figure a, upper line) were spiked into 1 mL healthy donor's whole blood. The results (Figure b, left column) demonstrated that the cancer cell isolation efficiency was around 80%. Secondly, 100 DAPI-stained MCF-7 cells (Figure a, lower line), which had lower EpCAM expression, were also spiked into 1 mL healthy donor's whole blood. MCF-7 cells exhibited slightly lower isolation efficiency (76%, Figure b, right column). The cell isolating efficiency was calculated by diving isolated cells by total spiked cells. Data are expressed as the mean ± SD from 3 independent assays.

Supplementary Figure S8

Specificities of CK19 against breast cancer cells and CK20 against colorectal cancer cells
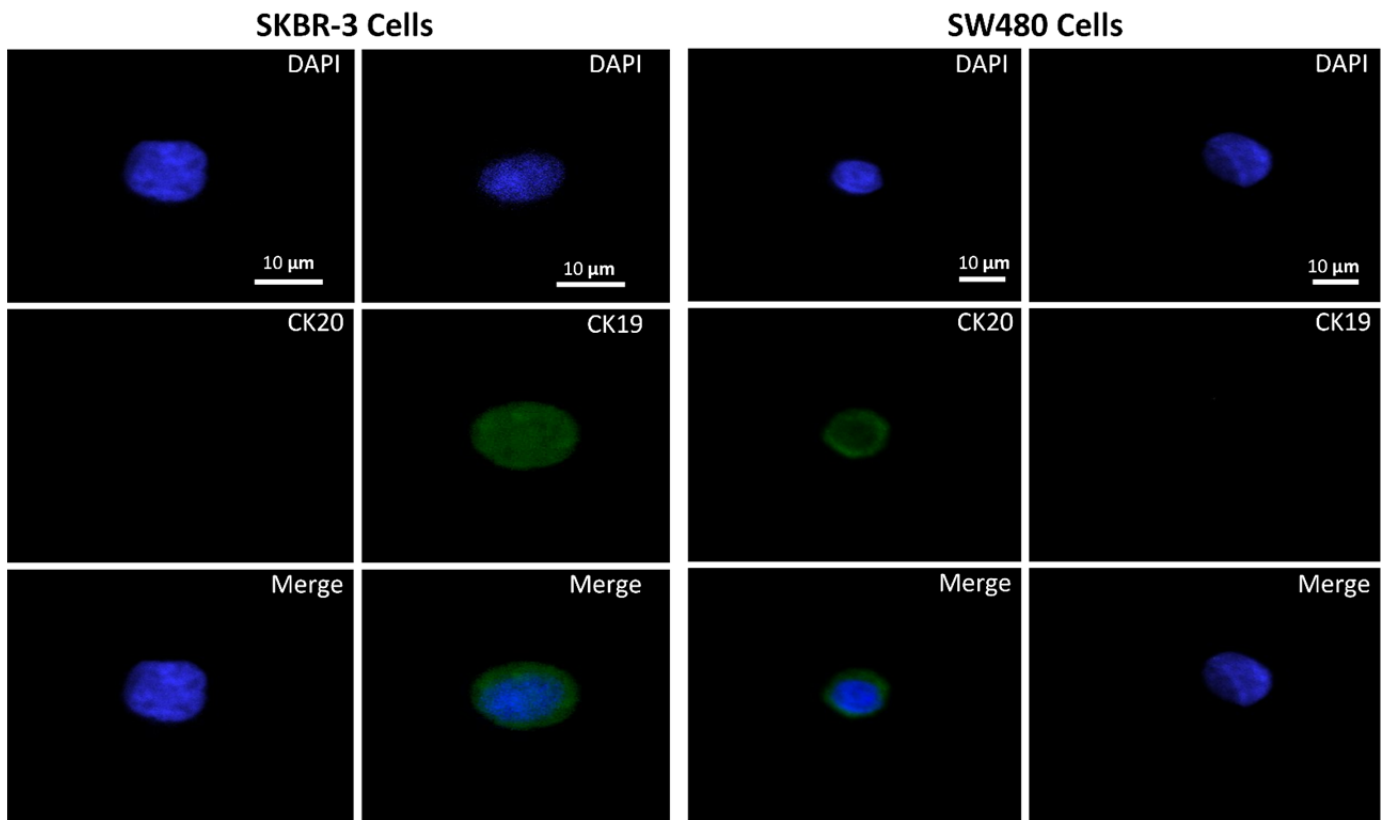
For different cancer types, different kinds of CK antibodies were used to identify CTCs. CK19-FITC antibody recognizes the SKBR-3 (human breast cancer) cells, not SW480 (human colorectal cancer) cells. CK20-FITC antibody recognizes the SW480 (human colorectal cancer) cells, not SKBR-3 (human breast cancer) cells. Blue spots represent the cell nucleic stained by DAPI while greed spots represent the CK-FITC antibodies which recognizing corresponding CK protein expressed on cell membrane.

Supplementary Figure S9
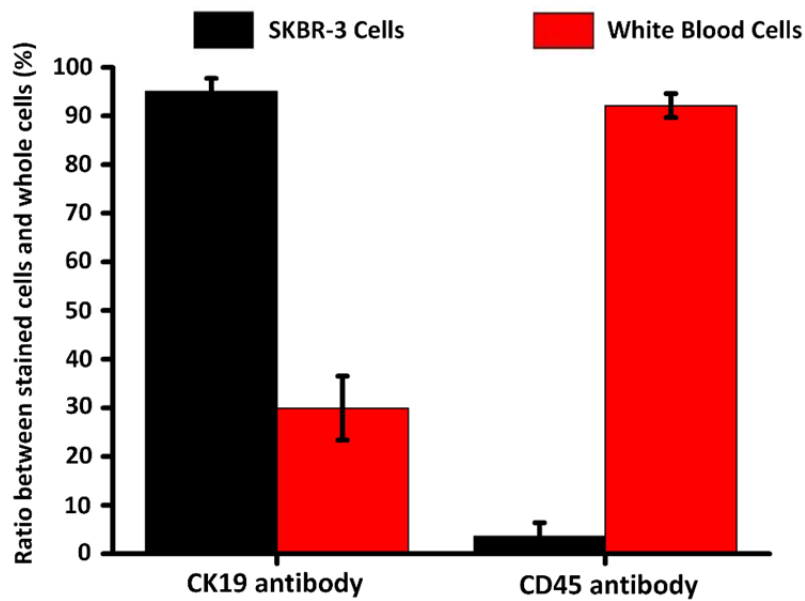
The CK19 and CD45 antibodies from diverse providers may exhibit fluctuation on its specificity, and eventually affect the accuracy of the CTC identification. Before each experiment, we evaluated the specificities of CK19 against SKBR-3 cells and CD45 against white blood cells. For the specificity evaluation of CK19, we immune-stained SKBR-3 cells and white blood cells by DAPI and CK19-FITC antibody. Then all cells were fluorescently imaged. We evaluated the specificity of CK19 by dividing CK19-FITC labelled SKBR-3 cells by total measured SKBR-3 cells and non-specificity of CK19 by dividing CK19-FITC labelled white blood cells by total measured white blood cells. Similarly, we evaluated the specificity of CD45 by dividing CD45-PE labelled white blood cells by total measured white blood cells and non-specificity of CD45 by dividing CD45-PE labelled SKBR-3 cells by total measured SKBR-3 cells. Data are expressed as the mean ± SD from 3 independent assays.

Supplementary Figure S10

Fluorescence quenching of CD45-PE and CK19-FITC
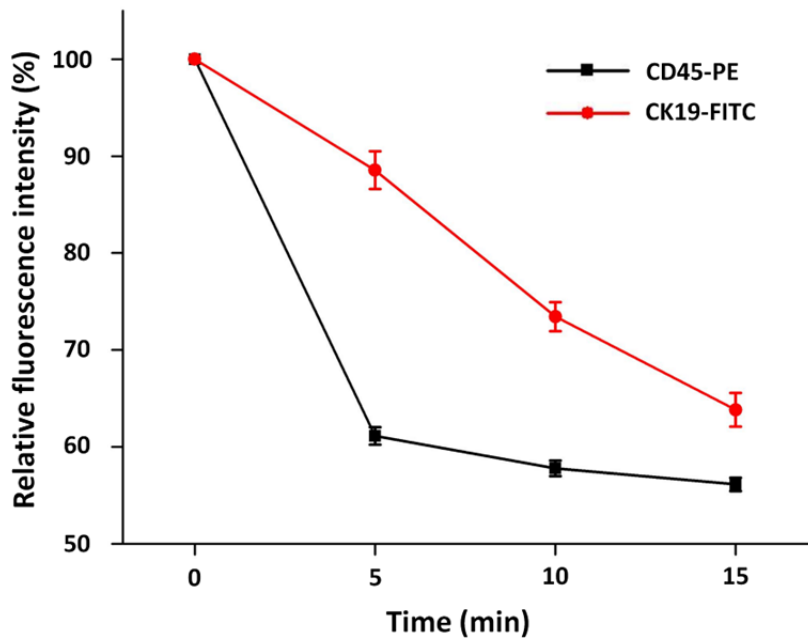
Just as other fluorescent dyes, the fluorescence of PE and FITC would be weakened, and eventually quenched while imaging. While imaging the whole chip, the fluorescence quenching would inevitably affect the accuracy of the CTC identification. We evaluated the fluorescence quenching of PE and FITC by measuring their fluorescence intensities on CD45-PE labelled white blood cells and CK19-FITC labelled SKBR-3 cells. For 5 minutes, the fluorescence intensity of PE and FITC reduced by 40% and 10%, respectively. After 15 minutes, both PE and FITC showed about 40% drop of fluorescence intensity. Data are expressed as the mean ± SD from 3 independent assays.

Supplementary Table S11

Patient and healthy donor information

| Patients All female	Age	Stage	TNM Status	ER Status	PR Status	Her2 Status	Notes
1	55	IIIc	pT1N3M0	++	++	+	first-line chemotherapy
2	47	IIIb	pT2N2M0	-	-	+	fourth-line chemotherapy
3	66	IIIc	pT2N3M0	-	-	+++	second-line chemotherapy
4	43	IV	cT1N3M1	+++	+++	++	multi-metastases at first-treatment
5	63	IIa	pT2N0M0	+++	++	++	second-line chemotherapy
6	61	IIb	pT2N1M0	+	+	-	second-line chemotherapy

2 healthy donors, a 43 years old female and a 47 years old male

Supplementary Figure S12

Identified CTCs from clinical blood samples
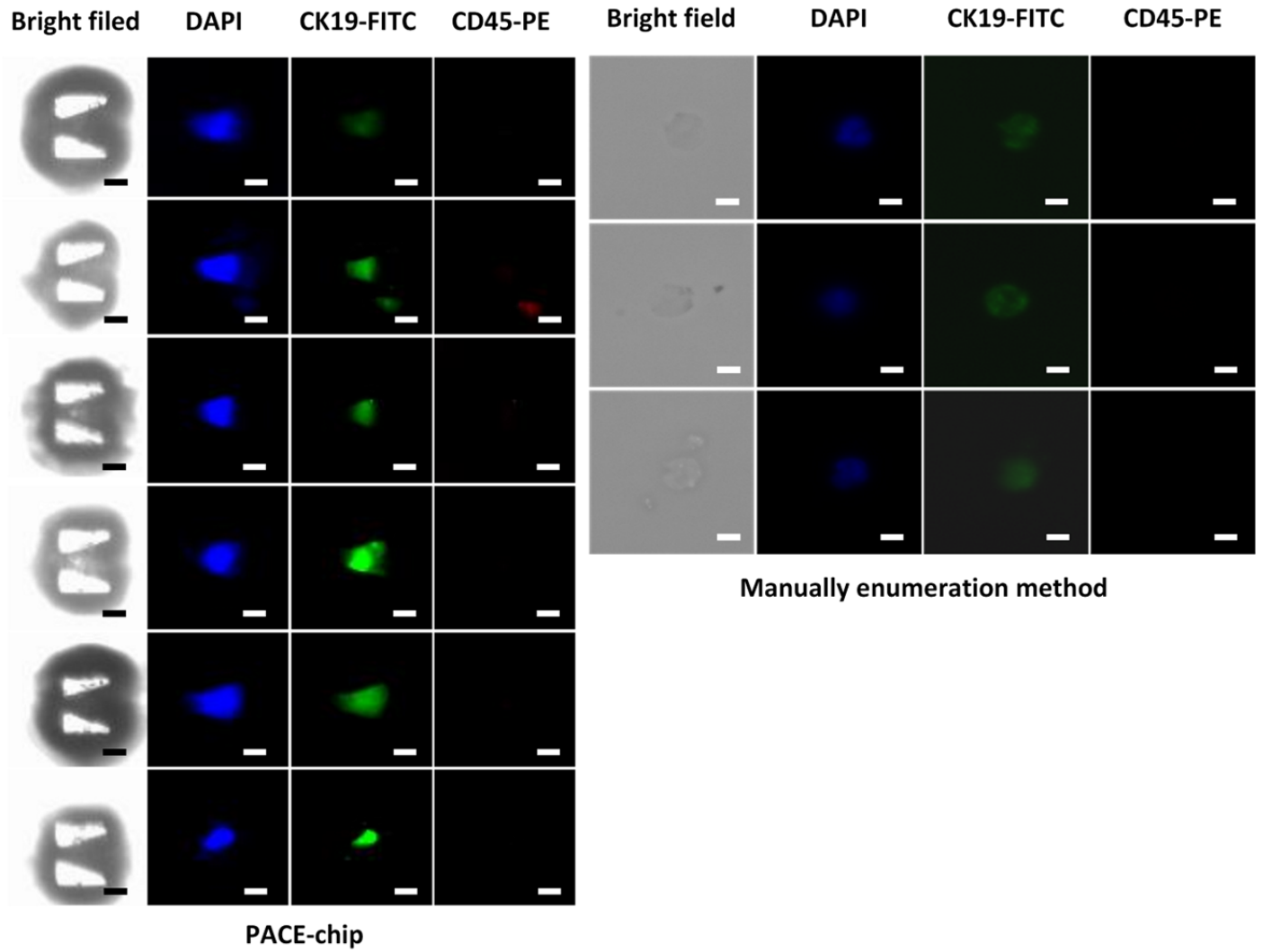
(a)
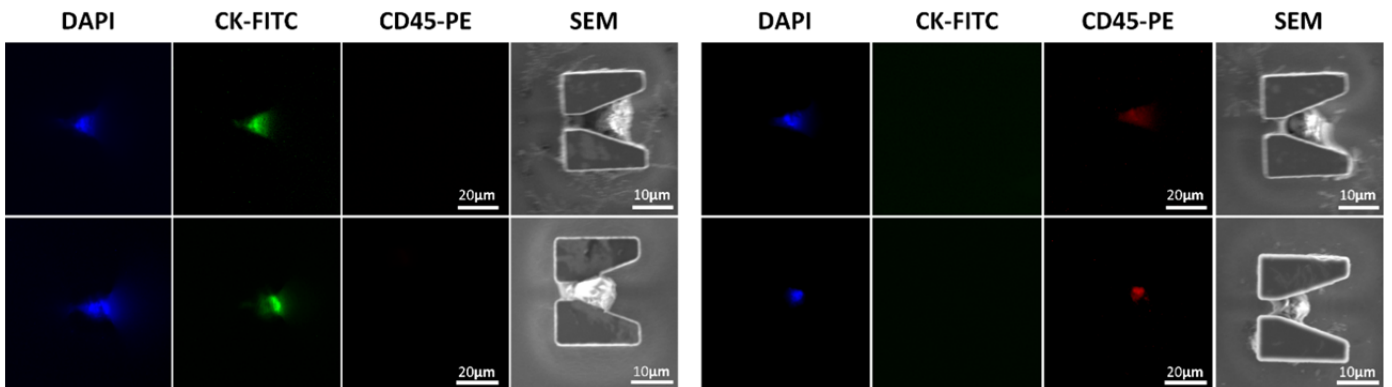
(b)

(a) We compared the automatic CTC enumeration and traditional tube-based CTC isolation combined with manually identification. We took 4 mL blood from a patient, and then divided it into 2 equal parts. 2 mL was treated by automatic CTC enumeration while the other 2 mL was manually examined using tube-based isolation. All identified CTCs from both assays were listed. 6 CTCs were found by automatic CTC enumeration while only 3 were found by manually identification. The blue spots represent cell nucleic. The green spots indicate cancer cells. The red color means white blood cells. A genuine CTC should exhibit blue and green, not red. Scale bars: 10 µm.

(b) Two identified CTCs (left) with DAPI+/CK19+/CD45- and two WBCs (right) with DAPI+/CK19-/CD45+ exhibit intact cell profiles in high-resolution SEM images. The patient is a 41 years old female, with stage IIA breast cancer, receiving third-line chemotherapy.

References

1. Karabacak NM, Spuhler PS, Fachin F, Lim EJ, Pai V, Ozkumur E, et al. Microfluidic, marker-free isolation of circulating tumor cells from blood samples. Nat Protocol. 2014; 9: 694-710.

2. Yoon HJ, Kim TH, Zhang Z, Azizi E, Pham TM, Paoletti C, et al. Sensitive capture of circulating tumour cells by functionalized graphene oxide nanosheets. Nat Nano. 2013; 8: 735-41.

3. Zhao M, Schiro PG, Kuo JS, Koehler KM, Sabath DE, Popov V, et al. An automated high-throughput counting method for screening circulating tumor cells in peripheral blood. Anal Chem. 2013; 85: 2465-71.